

XIV International Conference on Computational Plasticity. Fundamentals and Applications
COMPLAS XIV
E. Oñate, D.R.J. Owen, D. Peric & M. Chiumenti (Eds)

CRACK PHASE-FIELD MODELING OF ANISOTROPIC RUPTURE IN FIBROUS SOFT TISSUES

O. GÜLTEKİN¹, H. DAL² AND G.A. HOLZAPFEL^{1,3}

¹Institute of Biomechanics, Graz University of Technology
Stremayrgasse 16/II, 8010, Graz, Austria
e-mail: {gueltekin|holzapfel}@tugraz.at, web page: <http://www.biomech.tugraz.at/>

²Department of Mechanical Engineering, Middle East Technical University
Dumlupınar Bulvarı No. 1, Çankaya, 06800, Ankara, Turkey
e-mail: dal@metu.edu.tr, web page: <http://www.me.metu.edu.tr/meweb/>

³Faculty of Engineering Science and Technology
Norwegian University of Science and Technology (NTNU), 7491 Trondheim, Norway
e-mail: gerhard.holzapfel@ntnu.no, web page: <https://www.ntnu.no/ansatte/gerhard.holzapfel>

Key words: Fracture, Crack phase-field, Failure criteria, Fibrous soft tissue, Aorta

Abstract. The estimation of rupture in fibrous soft tissues has emerged as a central task in medical monitoring and risk assessment of diseases such as aortic dissection and aneurysms. In an attempt to address the challenges we have established a computational framework within the context of crack phase-field modeling and proposed an energy-based anisotropic failure criterion based on the distinction of isotropic and anisotropic material responses. Numerically we compare that criterion with other anisotropic failure criteria, in particular we analyze their capability to describe an admissible failure surface and how a crack can be propagated. A canonical rate-dependent setting of the crack phase-field model is formulated and solved in a weak sense by a standard Galerkin procedure featuring a one-pass operator-splitting algorithm on the temporal side. The anisotropic failure criteria are tested according to their performance on reflecting an admissible initiation, and crack propagation with an emphasis placed upon the aortic dissection.

1 INTRODUCTION

Rupture of fibrous soft tissues involves tangled series of coupled biomechanical processes imposing conspicuous limits on computational models to characterize physically relevant failure. In this respect, mathematical models can help physicians to better assess the risk of rupture involved in diseases such as aneurysms (Humphrey and Holzapfel [7]). In an attempt to address the related issues we have established a mathematical framework within the context of crack phase-field and proposed a novel energy-based failure criterion based on a distinction of isotropic and anisotropic material responses (Gültekin et al. [3]).

To date several contributions on failure criteria have been reported in the literature for both isotropic and anisotropic materials, see, e.g., Hill [5] and Tsai and Wu [13]. However, an account on their numerical performance, i.e. their capability to describe an admissible failure surface and a crack propagation, is not yet presented, the main objective of this communication. An anisotropic phase-field approach is formulated, enforcing the crack growth along the direction of fibers. A rate-dependent setting of the crack phase-field formulation is proposed which not only enhances the algorithmic stability upon macro-cracking but also becomes physically justifiable as, e.g., the aortic dissection is observed to be rate-dependent (Tong et al. [12]).

2 THEORY

This section deals with phase-field modeling of fracture in solids at finite strains featuring the primary field variables, namely the deformation map φ and the crack phase-field d in relation to the balance of linear momentum and the crack evolution, respectively.

2.1 The primary field variables of the multi-field problem

The coupled problem of fracture is described by φ and d , i.e.

$$\varphi_t(\mathbf{X}) : \begin{cases} \mathcal{B} \times \mathcal{T} & \rightarrow \mathcal{S}, \\ (\mathbf{X}, t) & \mapsto \mathbf{x} = \varphi(\mathbf{X}, t), \end{cases} \quad d : \begin{cases} \mathcal{B} \times \mathcal{T} & \rightarrow [0, 1], \\ (\mathbf{X}, t) & \mapsto d(\mathbf{X}, t), \end{cases} \quad (1)$$

where φ maps a material point $\mathbf{X} \in \mathcal{B} \subset \mathbb{R}^3$ in the reference configuration onto $\mathbf{x} \in \mathcal{S} \subset \mathbb{R}^3$ located in the spatial configuration, while the crack phase-field d interpolates between the intact ($d = 0$) and the ruptured ($d = 1$) state of the material. A key aspect is to provide a diffusive crack topology by smearing out the sharp crack surface over a solid domain using the length-scale parameter l (Miehe et al. [10, 8]). The sharp crack surface topology at time t can be denoted by $\Gamma(t) \subset \mathbb{R}^2$ in the solid \mathcal{B} , with the definition $\Gamma(d) = \int_{\Gamma} dA$. In contrast, a diffusive crack simply approximates the sharp crack surface by a volume integral in the form of the regularized crack surface functional

$$\Gamma_l(d) = \int_{\mathcal{B}} \gamma(d, \nabla d) dV, \quad \gamma(d, \nabla d) = \frac{1}{2l}(d^2 + l^2|\nabla d|^2), \quad (2)$$

where $\nabla[\bullet]$ denotes the gradient operator with respect to the reference coordinates, and γ is the isotropic volume-specific crack surface. This can be extended to a class of anisotropic materials via the introduction of an anisotropic volume-specific crack surface γ up to first order, i.e.

$$\gamma(d, \mathbf{Q} \star \nabla d) = \gamma(d, \nabla d), \quad \forall \mathbf{Q} \in \mathcal{G} \subset \mathcal{O}(3), \quad (3)$$

where \mathbf{Q} denotes the rotations in the symmetry group \mathcal{G} , a subset of the orthogonal group $\mathcal{O}(3)$ containing rotations and reflections, and \star denotes a transformation operator. The anisotropy is accounted by a second-order structure tensor \mathcal{L} such that

$$\mathcal{L} = l^2[\mathbf{I} + \omega_{\mathbf{M}}(\mathbf{M} \otimes \mathbf{M}) + \omega_{\mathbf{M}'}(\mathbf{M}' \otimes \mathbf{M}')], \quad (4)$$

which aligns the evolution of the crack according to the orientation of fibers in the continuum using the anisotropy parameters ω_M and $\omega_{M'}$ that regulate the transition from weak to strong anisotropy. The anisotropic volume-specific crack surface can now be represented by the alternative form

$$\gamma(d, \nabla d; \mathcal{L}) = \frac{1}{2l}(d^2 + \nabla d \cdot \mathcal{L} \nabla d). \quad (5)$$

2.2 Kinematics

The fundamental deformation measure at finite strain kinematics is the deformation gradient, i.e.

$$\mathbf{F} = \nabla \varphi. \quad (6)$$

Manifolds are equipped with the covariant reference metric tensor \mathbf{G} and the spatial metric tensor \mathbf{g} transforming the co and contravariant objects in the Lagrangian and Eulerian manifolds, respectively. Exploiting the multiplicative decomposition of \mathbf{F} into a volumetric part \mathbf{F}_{vol} and an isochoric part $\bar{\mathbf{F}}$, with $\det \bar{\mathbf{F}} = 1$, we have

$$\mathbf{F} = \mathbf{F}_{\text{vol}} \bar{\mathbf{F}} \quad \text{with} \quad \mathbf{F}_{\text{vol}} = J^{1/3} \mathbf{I}, \quad \bar{\mathbf{F}} = J^{-1/3} \mathbf{F}, \quad (7)$$

where the Jacobian $J = \det \mathbf{F} > 0$ characterizes the volume map of an infinitesimal reference volume element onto the associated spatial element. Subsequently, we define the unimodular part of the left Cauchy-Green tensor $\bar{\mathbf{b}}$ and its first invariant \bar{I}_1 as

$$\bar{\mathbf{b}} = \bar{\mathbf{F}} \mathbf{G}^{-1} \bar{\mathbf{F}}^T, \quad \bar{I}_1 = \text{tr} \bar{\mathbf{b}}. \quad (8)$$

The anisotropic structure of fibrous soft tissues makes it necessary to consider additional invariants. Hence, we introduce two reference unit vectors \mathbf{M} and \mathbf{M}' representing the mean fiber orientations, with their spatial counterparts $\mathbf{m} = \mathbf{F} \mathbf{M}$ and $\mathbf{m}' = \mathbf{F} \mathbf{M}'$ idealizing the micro-structure. Following this, we describe the additional invariants

$$I_4 = \mathbf{g} : (\mathbf{m} \otimes \mathbf{m}), \quad I_6 = \mathbf{g} : (\mathbf{m}' \otimes \mathbf{m}'), \quad (9)$$

expressed by the structure tensors $\mathbf{A}_{\mathbf{m}} = \mathbf{m} \otimes \mathbf{m}$ and $\mathbf{A}_{\mathbf{m}'} = \mathbf{m}' \otimes \mathbf{m}'$.

2.3 Constitutive modeling of artery walls

The effective Helmholtz free-energy function Ψ_0 describes the local anisotropic mechanical response of the intact solid. We assume a specific form which comprises the effective volumetric part U_0 , the isotropic part Ψ_0^{iso} and the anisotropic part Ψ_0^{ani} according to

$$\Psi_0(\mathbf{g}, \mathbf{F}, \mathbf{A}_{\mathbf{m}}, \mathbf{A}_{\mathbf{m}'}) = U_0(J) + \Psi_0^{\text{iso}}(\mathbf{g}, \bar{\mathbf{F}}) + \Psi_0^{\text{ani}}(\mathbf{g}, \mathbf{F}, \mathbf{A}_{\mathbf{m}}, \mathbf{A}_{\mathbf{m}'}), \quad (10)$$

in the sense of Dal [1]. It needs to be underlined that in (10) the multiplicative decomposition of \mathbf{F} is only used upon the matrix response; in other words, we omit the multiplicative decomposition of \mathbf{F} for the fiber response. The effective volumetric part is given by

$$U_0(J) = \kappa(J - \ln J - 1), \quad (11)$$

while Ψ_0^{iso} and Ψ_0^{ani} are functions of the invariants according to

$$\Psi_0^{\text{iso}}(\mathbf{g}, \bar{\mathbf{F}}) = \hat{\Psi}_0^{\text{iso}}(\bar{I}_1), \quad \Psi_0^{\text{ani}}(\mathbf{g}, \mathbf{F}, \mathbf{A}_m, \mathbf{A}_{m'}) = \hat{\Psi}_0^{\text{ani}}(I_4, I_6), \quad (12)$$

which take on the neo-Hookean and exponential models according to Holzapfel et al. [6]

$$\hat{\Psi}_0^{\text{iso}}(\bar{I}_1) = \frac{\mu}{2}(\bar{I}_1 - 3), \quad \hat{\Psi}_0^{\text{ani}}(I_4, I_6) = \frac{k_1}{2k_2} \sum_{i=4,6} \{\exp[k_2(I_i - 1)^2] - 1\}, \quad (13)$$

representing the elastic response of the ground matrix and the two distinct families of collagen fibers, respectively. To give an account of the parameters, κ denotes the bulk modulus in (11), while μ indicates the shear modulus in (13)₁. The parameters k_1 and k_2 in (13)₂ denote a stress-like and a dimensionless parameter, respectively. The anisotropic part contributes to the mechanical response only when a family of fibers is under extension, i.e. $I_4 > 1$ and $I_6 > 1$ [6]. The derivations of the corresponding constitutive response, i.e. the effective Kirchhoff stress tensor $\boldsymbol{\tau}_0$ and the effective elasticity tensor \mathbb{C}_0 can be found in Gültekin et al. [4].

2.4 Variational formulation based on power balance

For a degrading anisotropic solid with two families of fibers, the Helmholtz free-energy function Ψ can be written as

$$\Psi(\mathbf{g}, \mathbf{F}, \mathbf{A}_m, \mathbf{A}_{m'}; d) = g(d)\Psi_0(\mathbf{g}, \mathbf{F}, \mathbf{A}_m, \mathbf{A}_{m'}), \quad (14)$$

where Ψ_0 is the effective free energy of the hypothetically intact solid according to (10). The explicit form of the monotonically decreasing quadratic degradation function g is

$$g(d) = (1 - d)^2, \quad (15)$$

which describes the degradation of the solid as d evolves, along with appropriate growth conditions [2, 3, 4]. Hence, the volumetric, isotropic and anisotropic parts of the free-energy function $\Psi = U + \hat{\Psi}^{\text{iso}} + \hat{\Psi}^{\text{ani}}$ for a degenerating material become

$$U(J, d) = g(d)U_0(J), \quad \hat{\Psi}^{\text{iso}}(\bar{I}_1; d) = g(d)\hat{\Psi}_0^{\text{iso}}(\bar{I}_1), \quad \hat{\Psi}^{\text{ani}}(I_4, I_6; d) = g(d)\hat{\Psi}_0^{\text{ani}}(I_4, I_6), \quad (16)$$

respectively. We now write the rate of the energy storage functional \mathcal{E} by considering the time derivative of the isotropic and the anisotropic contributions of (16)_{2,3} integrated over the domain, i.e.

$$\mathcal{E}(\dot{\boldsymbol{\varphi}}, \dot{d}; \boldsymbol{\varphi}, d) = \int_{\mathcal{B}} (\boldsymbol{\tau} : \mathbf{g}\nabla_x \dot{\boldsymbol{\varphi}} - f\dot{d})dV, \quad (17)$$

where $\nabla_x[\bullet]$ denotes the gradient operator with respect to the spatial coordinates. We have defined the Kirchhoff stress tensor $\hat{\boldsymbol{\tau}}$ and the energetic force f such that

$$\boldsymbol{\tau} = g(d)(\boldsymbol{\tau}_0^{\text{iso}} + \boldsymbol{\tau}_0^{\text{ani}}), \quad f = -\partial_d[U(J, d) + \hat{\Psi}^{\text{iso}}(\bar{I}_1; d) + \hat{\Psi}^{\text{ani}}(I_4, I_6; d)], \quad (18)$$

where $\boldsymbol{\tau}$ is essentially obtained via the effective isotropic and anisotropic Kirchhoff stresses $\boldsymbol{\tau}_0^{\text{iso}}$ and $\boldsymbol{\tau}_0^{\text{ani}}$, respectively. Meanwhile, f can be interpreted as the work conjugate quantity to \dot{d} . The external action on the body gives the external power functional \mathcal{P} , i.e.

$$\mathcal{P}(\dot{\boldsymbol{\varphi}}) = \int_{\mathcal{B}} \rho_0 \tilde{\boldsymbol{\gamma}} \cdot \dot{\boldsymbol{\varphi}} dV + \int_{\partial \mathcal{B}_t} \tilde{\mathbf{t}} \cdot \dot{\boldsymbol{\varphi}} da, \quad (19)$$

where ρ_0 , $\tilde{\boldsymbol{\gamma}}$ and $\tilde{\mathbf{t}}$ represent the material density, the prescribed body force and the spatial surface traction, respectively. In what follows, the dissipation functional \mathcal{D} accounts for the dissipated energy in the body is given as

$$\mathcal{D}(\dot{d}) = \int_{\mathcal{B}} g_c[\delta_d \gamma(d, \nabla d; \mathcal{L})] \dot{d} dV, \quad (20)$$

where $\delta_d \gamma$ defines the variational derivative of the volume-specific crack surface γ , whereas g_c is the critical fracture energy (Griffith-type critical energy release rate), see Miehe et al. [10, 8] and Gültekin et al. [3].

Concerning thermodynamics, \mathcal{D} has to be non-negative for all admissible deformation processes, a primary demand of the second law of thermodynamics. This inequality is *a priori* fulfilled by a the local form of (20) featuring a positive and convex propensity (Miehe et al. [10]). The local form of (20) can be stated by the principle of maximum dissipation via the following constrained optimization problem

$$g_c[\delta_d \gamma(d, \nabla d; \mathcal{L})] \dot{d} = \sup_{\beta \in \mathbb{E}} \beta \dot{d}, \quad (21)$$

which can be solved by a Lagrange method yielding

$$g_c[\delta_d \gamma(d, \nabla d; \mathcal{L})] \dot{d} = \sup_{\beta, \lambda \geq 0} [\beta \dot{d} - \lambda t_c(\beta; d, \nabla d)], \quad (22)$$

where the local driving force β , dual to \dot{d} , and the Lagrange multiplier λ enforce the constraint. In addition, the threshold function t_c delineating a reversible domain \mathbb{E} is

$$\mathbb{E}(\beta) = \{\beta \in \mathbb{R} \mid t_c(\beta; d, \nabla d) = \beta - g_c[\delta_d \gamma(d, \nabla d; \mathcal{L})] \leq 0\}. \quad (23)$$

Finally, the extended dissipation functional \mathcal{D}_λ reads

$$\mathcal{D}_\lambda(\dot{d}, \beta, \lambda; d) = \int_{\mathcal{B}} [\beta \dot{d} - \lambda t_c(\beta; d, \nabla d)] dV. \quad (24)$$

2.4.1 Mixed rate-independent variational formulation based on power balance

The sum of the functionals (17), (19) and (24) describes a rate-type potential giving rise to the power balance, i.e.

$$\Pi_\lambda = \mathcal{E} + \mathcal{D}_\lambda - \mathcal{P}. \quad (25)$$

On the basis of the rate-type potential (25), the mixed saddle point principle for the quasi-static process states

$$\{\dot{\varphi}, \dot{d}, \beta, \lambda\} = \text{Arg} \left\{ \inf_{\dot{\varphi} \in \mathcal{W}_{\dot{\varphi}}} \inf_{\dot{d} \in \mathcal{W}_{\dot{d}}} \sup_{\beta, \lambda \geq 0} \Pi_{\lambda} \right\}, \quad (26)$$

with the admissible domains for the primary variables $\mathcal{W}_{\dot{\varphi}} = \{\dot{\varphi} \mid \dot{\varphi} = \mathbf{0} \text{ on } \partial\mathcal{B}_{\varphi}\}$ and $\mathcal{W}_{\dot{d}} = \{\dot{d} \mid \dot{d} = 0 \text{ on } \partial\mathcal{B}_d\}$. By considering the variation of Π_{λ} we obtain the Euler-Lagrange equations describing the mixed multi-field problem for the rate-independent fracture of an anisotropic hyperelastic solid, i.e.

$$\boxed{\begin{aligned} 1: & \quad J \text{div}(J^{-1} \boldsymbol{\tau}) + \rho_0 \tilde{\boldsymbol{\gamma}} = \mathbf{0}, \\ 2: & \quad \beta - f = 0, \\ 3: & \quad \dot{d} - \lambda = 0, \end{aligned}} \quad (27)$$

along with the Karush-Kuhn-Tucker-type loading-unloading conditions ensuring the principal of maximum dissipation in case of an evolution of the crack phase-field parameter d , i.e. $\lambda \geq 0$, $t_c \leq 0$ and $\lambda t_c = 0$.

2.4.2 A mixed rate-dependent variational formulation based on power balance

Now we deal with the viscous extension of the variational approach and introduce a Perzyna-type viscous extension of \mathcal{D} such that

$$\mathcal{D}_{\eta}(\dot{d}, \beta; d) = \int_B \left[\beta \dot{d} - \frac{1}{2\eta} \langle t_c(\beta; d, \nabla d) \rangle^2 \right] dV, \quad (28)$$

where the viscosity η determines the viscous over-force governing the evolution of \dot{d} . In (28) the positive values for the threshold function t_c are filtered out by the ramp function $\langle x \rangle = (x + |x|)/2$. The corresponding viscous rate-type potential reads

$$\Pi_{\eta} = \mathcal{E} + \mathcal{D}_{\eta} - \mathcal{P}. \quad (29)$$

On the basis of the rate-type potential (29), we establish a mixed saddle point principle for the quasi-static process, i.e.

$$\{\dot{\varphi}, \dot{d}, \beta\} = \text{Arg} \left\{ \inf_{\dot{\varphi} \in \mathcal{W}_{\dot{\varphi}}} \inf_{\dot{d} \in \mathcal{W}_{\dot{d}}} \sup_{\beta \geq 0} \Pi_{\eta} \right\}, \quad (30)$$

with the admissible domains for the primary state variables. One can retrieve the coupled set of Euler-Lagrange equations for the rate-dependent fracture by simply taking the variation of Π_{η} , i.e.

$$\boxed{\begin{aligned} 1: & \quad J \text{div}(J^{-1} \boldsymbol{\tau}) + \rho_0 \tilde{\boldsymbol{\gamma}} = \mathbf{0}, \\ 2: & \quad \beta - f = 0, \\ 3: & \quad \dot{d} - \langle t_c(\beta; d, \nabla d) \rangle / \eta = 0, \end{aligned}} \quad (31)$$

The explicit form of the threshold function t_c recasts the equality (31)₃ in the form

$$f = \eta \dot{d} + g_c \delta_d \gamma(d, \nabla d). \quad (32)$$

2.5 Crack driving function and failure Ansatz

Focusing on the rate-independent case in (32), where $\eta \rightarrow 0$, we elaborate on the energetic force (18)₂. Accordingly, we substitute (15) and (16) into (18)₂ to arrive at

$$f = 2(1 - d)(U_0 + \hat{\Psi}_0^{\text{iso}} + \hat{\Psi}_0^{\text{ani}}) = 2(1 - d)\Psi_0. \quad (33)$$

By substituting (33) into (32) for the rate-independent case we obtain (the calculation of the variational derivative can be found in Gültekin et al. [3])

$$2(1 - d)\frac{\Psi_0}{g_c/l} = d - \nabla \cdot (\mathcal{L}\nabla d). \quad (34)$$

With this notion at hand, we can define the dimensionless crack driving function

$$\boxed{\bar{\mathcal{H}} = \frac{\Psi_0}{g_c/l}.} \quad (35)$$

As discussed in Miehe et al. [9] the dimensionless characteristics of $\bar{\mathcal{H}}$ allows the incorporation of different failure criteria. A particular form of the failure Ansatz is postulated in accordance with two significant conditions, i.e. the irreversibility of the crack and the positiveness of $\bar{\mathcal{H}}$ ensuring that the crack growth solely takes place upon loading, i.e.

$$\boxed{\mathcal{H}(t) = \max_{s \in [0, t]} [\langle \bar{\mathcal{H}}(s) - 1 \rangle].} \quad (36)$$

With these adjustments (34) takes on the following form

$$\boxed{2(1 - d)\mathcal{H} = d - \nabla \cdot (\mathcal{L}\nabla d).} \quad (37)$$

Bearing this in mind, we recall the rate-dependent case for $\eta \neq 0$, i.e.

$$\boxed{2(1 - d)\mathcal{H} = d - \nabla \cdot (\mathcal{L}\nabla d) + \eta \dot{d},} \quad (38)$$

which compares to (32) with the replacement of the dimensional energetic force by the dimensionless failure Ansatz, the cornerstone of the crack phase-field modeling.

2.6 Anisotropic failure criteria

The dimensionless crack driving function (35) already reflects an energy-based criterion for a general isotropic material. However, we know that most fibrous soft tissues exhibit an anisotropic morphology, thereby an anisotropic mechanical response is expected. We, therefore, provide a short description of anisotropic failure criteria which may manifest the rupture phenomena in coherence with clinical observations. For simplicity, the ensuing formulations are established according to the assumption that the principal axes of anisotropy lie on the axes of reference. Nonetheless, transformation of stress components can be achieved without much effort [4].

2.6.1 Energy-based anisotropic failure criterion

Two distinct failure processes are assumed to govern rupture of the ground matrix and the fibers as suggested by Gültekin et al. [3]. Accordingly, the energetic force (18)₂ can be additively decomposed into an isotropic part f_{iso} and an anisotropic part f_{ani} such that

$$f_{\text{iso}} = 2(1 - d)(U_0 + \hat{\Psi}_0^{\text{iso}}), \quad f_{\text{ani}} = 2(1 - d)\hat{\Psi}_0^{\text{ani}}, \quad (39)$$

which, in their turn, modify (34) into two distinct fracture processes which are

$$(1 - d)\bar{\mathcal{H}} = d - \frac{1}{2}\nabla \cdot (\mathcal{L}\nabla d), \quad \text{with} \quad \bar{\mathcal{H}} = \bar{\mathcal{H}}^{\text{iso}} + \bar{\mathcal{H}}^{\text{ani}}, \quad (40)$$

where the dimensionless crack driving functions are defined as

$$\bar{\mathcal{H}}^{\text{iso}} = \frac{\hat{\Psi}_0^{\text{iso}}}{g_c^{\text{iso}}/l}, \quad \bar{\mathcal{H}}^{\text{ani}} = \frac{\hat{\Psi}_0^{\text{ani}}}{g_c^{\text{ani}}/l}. \quad (41)$$

Therein, g_c^{iso}/l and g_c^{ani}/l are the distinct critical fracture energies over the length scale for the ground matrix and for the fibers, respectively. Finally, we provide the modified forms of the rate-dependent and rate-independent cases for the crack evolution, i.e.

$$(1 - d)\mathcal{H} = d - \frac{1}{2}\nabla \cdot (\mathcal{L}\nabla d), \quad (1 - d)\mathcal{H} = d - \frac{1}{2}\nabla \cdot (\mathcal{L}\nabla d) + \eta\dot{d}. \quad (42)$$

For more details regarding the derivations see [3, 4].

2.6.2 Stress-based anisotropic Tsai-Wu failure criterion

The Tsai-Wu criterion is based on the strength of the material at which the stress space intercepts the assumed failure surface (Tsai and Wu [13]). Accordingly, the dimensionless crack driving function with respect to the effective Cauchy stress tensor $\boldsymbol{\sigma}_0$ assumes a composition of two scalar functions, i.e.

$$\bar{\mathcal{H}} = \mathbf{T} : \boldsymbol{\sigma}_0 + \boldsymbol{\sigma}_0 : \mathbb{T} : \boldsymbol{\sigma}_0, \quad (43)$$

where \mathbf{T} and \mathbb{T} denote the second and fourth-order strength tensors, respectively. Through assumptions and simplifications introduced by symmetry relations we end up with

$$T_{ii} = \frac{1}{(\sigma_i^u)^2} \quad (44)$$

for the diagonal terms of the fourth-order strength tensor related to ultimate normal and shear stresses σ_i^u , with $i \in \{1, \dots, 6\}$.

2.6.3 Stress-based anisotropic Hill failure criterion

Considered as the anisotropic extension of the von Mises–Huber criterion, the Hill criterion (Hill [5]) uses a quadratic form of $\overline{\mathcal{H}}$ such that

$$\overline{\mathcal{H}} = \boldsymbol{\sigma}_0^{\text{vm}} : \mathbb{T} : \boldsymbol{\sigma}_0^{\text{vm}}, \quad (45)$$

where $\boldsymbol{\sigma}_0^{\text{vm}}$ represents the effective von Mises stress tensor. The components of $\boldsymbol{\sigma}_0^{\text{vm}}$ can be defined in terms of general stress components, i.e.

$$\begin{aligned} \sigma_{0_1}^{\text{vm}} &= \sigma_{0_1} - \sigma_{0_2}, & \sigma_{0_2}^{\text{vm}} &= \sigma_{0_2} - \sigma_{0_3}, & \sigma_{0_3}^{\text{vm}} &= \sigma_{0_3} - \sigma_{0_1}, \\ \sigma_{0_4}^{\text{vm}} &= \sigma_{0_4}, & \sigma_{0_5}^{\text{vm}} &= \sigma_{0_5}, & \sigma_{0_6}^{\text{vm}} &= \sigma_{0_6}. \end{aligned} \quad (46)$$

The fourth-order strength tensor \mathbb{T} pertains to the effective normal stresses and shear stresses [4].

2.6.4 Principal stress criterion

Developed on the basis of principal stresses the criterion by Raina and Miehe [11] reports on the spectral decomposition of the effective Cauchy stress tensor and takes the positive principal stresses into account, i.e.

$$\boldsymbol{\sigma}_0^+ = \sum_{i=1}^3 \langle \sigma_{0_i} \rangle \mathbf{n}_i \otimes \mathbf{n}_i, \quad (47)$$

where σ_{0_i} denote the effective principal stresses, and \mathbf{n}_i are the corresponding eigenvectors for $i \in \{1, 2, 3\}$. Accordingly, $\overline{\mathcal{H}}$ is rewritten as

$$\overline{\mathcal{H}} = \boldsymbol{\sigma}_0^+ : \mathbb{T} : \boldsymbol{\sigma}_0^+, \quad (48)$$

where the fourth-order strength tensor \mathbb{T} reads in the index notation

$$(\mathbb{T})_{ijkl} = \frac{1}{4\sigma_{\text{crit}}^2} (A_{ik}A_{jl} + A_{il}A_{jk}), \quad (49)$$

where σ_{crit} denotes the reference critical stress associated with uniaxial loading in a certain axis that can be conceptually replaced by an ultimate stress. Therein, \mathbf{A} is expressed in index notation for $i, j, k, l \in \{1, 2, 3\}$, for which details are provided in [11].

3 NUMERICAL EXAMPLES

We now briefly demonstrate the performance of the proposed model applied to fracture of a fibrous soft tissue for which the crack initiation and propagation associated with different failure criteria are compared for simple yet representative numerical examples.

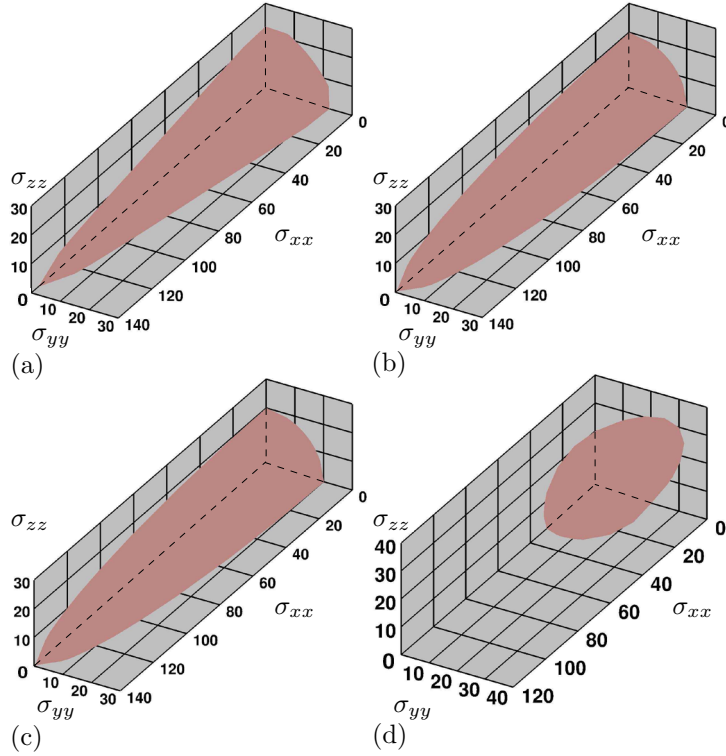


Figure 1: Failure surfaces in regard to Cauchy stresses σ_{xx} , σ_{yy} and σ_{zz} in kPa at which the failure conditions are satisfied, leading to $d > 0$ for (a) the energy-based; (b) the Tsai-Wu; (c) the maximum principal stress; (d) the Hill failure criterion (adopted from Gültekin et al. [4]).

3.1 Numerical investigation of the failure surfaces

The first example deals with the onset of micro-cracking with regard to distinct failure criteria, as mentioned in Section 2.6. The problem setup involves a homogeneous case with a unit cube discretized by one hexahedral element resolving the analytical solution for the deformation and stress. The sample, regarded as transversely isotropic, undergoes a series of uniaxial and biaxial deformations (for details see Gültekin et al. [4]).

Figures 1(a),(b) and (c) illustrate the resulting failure surfaces at the instance when $d \neq 0$ for the energy-based, Tsai-Wu and the principal stress criterion, respectively. The results conspicuously retrieve ellipsoidal failure surfaces. Figure 1(d) indicates the failure surface for the Hill criterion. In fact, this criterion induces surfaces diverging from being elliptic. In particular, the isotropic failure envelope on the yz -plane eventually becomes discernable, see Fig. 1(d), which recovers the von Mises–Huber criterion, as expected.

3.2 Peel test investigated with different failure criteria

The second example shows a peel test alluding to aortic dissection. This benchmark, with an initial tear, models a hypothetical artery comprised of a single family of fibers with orientation \mathbf{M} (again for more details see [4]).

The two arms of the strip are separated by an initial tear and pulled apart in opposite

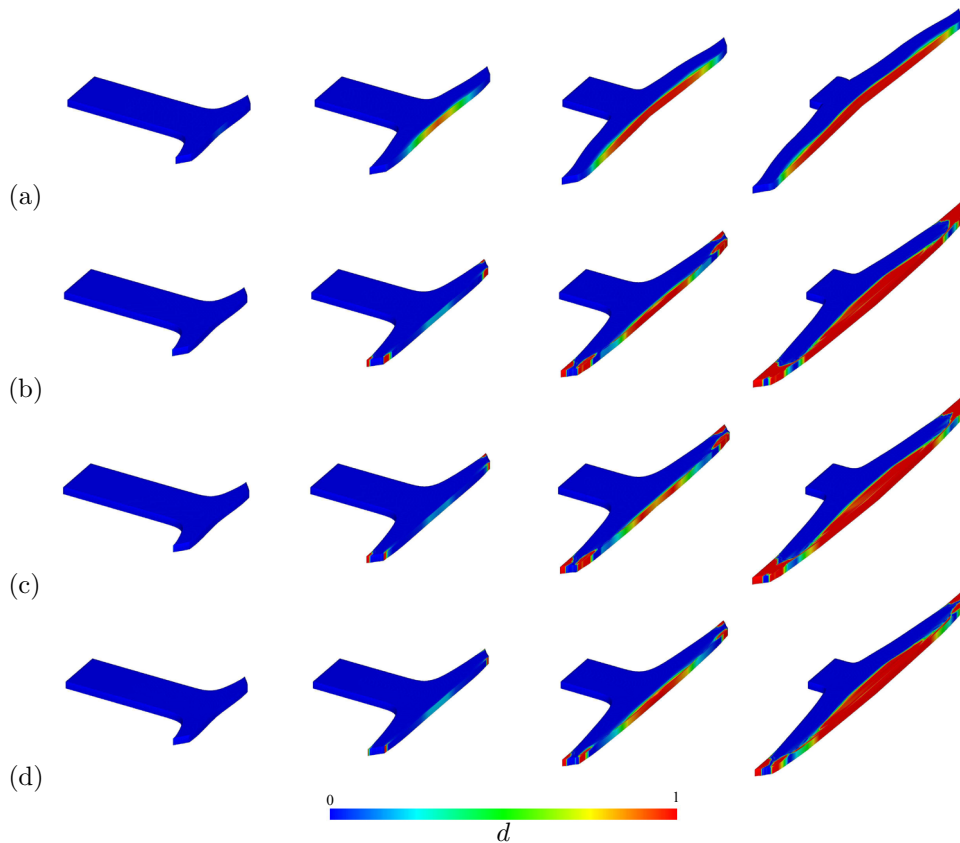


Figure 2: Evolution of the crack phase-field d for (a) the energy-based; (b) the Tsai-Wu; (c) the principal stress criterion, as the arterial tissue with an initial tear is being pulled in two opposite directions.

directions, see Fig. 2. Analysis results render the stress-based criteria susceptible to instabilities in terms of crack growth upon the initiation of macro-cracks in the material thereby the convergence of the algorithm becomes problematic. Moreover, the use of stress-based criteria leads to a crack propagation susceptible to boundary effects not observed in the case of the energy-based criterion.

4 CONCLUSION

A number of anisotropic failure criteria, essentially based on free energy or stress, was compared in terms of their capability to manifest admissible anisotropic failure surfaces and crack propagations for simple boundary-value problems (BVPs). On the theoretical side, the anisotropic crack phase-field model, established according to a continuous variational setup due to a power balance, provided the backbone of our modeling endeavors. On the numerical side, we focused on the failure surfaces of the used criteria induced for a homogeneous problem subjected to uniaxial and planar biaxial deformations. A peel test was also analyzed and the respective dissections were examined. Results favor the energetic-based criterion to accomplish a stable crack growth for the analyzed 3D BVPs blended with anisotropy at finite strains.

REFERENCES

- [1] H. Dal. Quasi-incompressible and quasi-inextensible element formulation for transversely anisotropic materials. *Int. J. Numer. Meth. Engng*, 2017. submitted.
- [2] O. Gültekin. A Phase Field Approach to the Fracture of Anisotropic Medium. Master's Thesis, University of Stuttgart, Institute of Applied Mechanics (CE), 2014.
- [3] O. Gültekin, H. Dal, and G. A. Holzapfel. A phase-field approach to model fracture of arterial walls: theory and finite element analysis. *Comput. Meth. Appl. Mech. Eng.*, 312:542–566, 2016.
- [4] O. Gültekin, H. Dal, and G. A. Holzapfel. Numerical aspects of anisotropic failure in soft biological tissues favor energy-based criteria: A rate-dependent mixed crack phase-field model. *Comput. Meth. Appl. Mech. Eng.*, 2017. submitted.
- [5] R. Hill. A theory of the yielding and plastic flow of anisotropic metals. *Proc. R. Soc. Lond. A*, 193:281–297, 1948.
- [6] G. A. Holzapfel, T. C. Gasser, and R. W. Ogden. A new constitutive framework for arterial wall mechanics and a comparative study of material models. *J. Elasticity*, 61:1–48, 2000.
- [7] J. D. Humphrey and G. A. Holzapfel. Mechanics, mechanobiology, and modeling of human abdominal aorta and aneurysms. *J. Biomech.*, 45:805–814, 2012.
- [8] C. Miehe, M. Hofacker, and F. Welschinger. A phase field model for rate-independent crack propagation: Robust algorithmic implementation based on operator splits. *Comput. Meth. Appl. Mech. Eng.*, 199:2765–2778, 2010.
- [9] C. Miehe, L.-M. Schänzel, and H. Ulmer. Phase field modeling of fracture in multi-physics problems. Part I. Balance of crack surface and failure criteria for brittle crack propagation in thermo-elastic solids. *Comput. Meth. Appl. Mech. Eng.*, 294:449–485, 2015.
- [10] C. Miehe, F. Welschinger, and M. Hofacker. Thermodynamically consistent phase-field models of fracture: Variational principles and multi-field FE implementations. *Int. J. Numer. Meth. Engng*, 83:1273–1311, 2010.
- [11] A. Raina and C. Miehe. A phase-field model for fracture in biological tissues. *Biomech. Model. Mechanobiol.*, 15:479–496, 2016.
- [12] J. Tong, T. Cohnert, P. Regitnig, J. Kohlbacher, R. Birner-Gruenberger, A. J. Schriebl, G. Sommer, and G. A. Holzapfel. Variations of dissection properties and mass fractions with thrombus age in human abdominal aortic aneurysms. *J. Biomech.*, 47:14–23, 2014.
- [13] S. W. Tsai and E. M. Wu. A general theory of strength of anisotropic materials. *J. Compos. Mater.*, 5:58–80, 1971.